Aust. J. Phys., 1995, **48**, 871–86

Hamiltonian Maps for Heliac Magnetic Islands

M. G. Davidson,[A] *R. L. Dewar, H. J. Gardner and J. Howard*

Department of Theoretical Physics and Plasma Research Laboratory,
Research School of Physical Sciences and Engineering,
Australian National University, Canberra, ACT 0200, Australia.
robert.dewar@anu.edu.au.
[A] Permanent address: Western Washington University,
Bellingham, WA 98225-9064, USA.
davidson@wwu.edu.

Abstract

Magnetic islands in toroidal heliac stellarator vacuum fields are explored with Hamiltonian chaos theory and the associated area-preserving maps. Magnetic field line island chains are examined first analytically, with perturbation theory, and then numerically to produce Poincaré sections, which are compared with H-1 Heliac stellarator puncture plot diagrams. Rotational transform profiles are chosen to permit the comparison of twist map and nontwist map predictions with field line behaviour computed by a field line tracing computer program and observed experimentally.

1. Introduction

The goal of this work is to examine the role of Hamiltonian chaos theory and associated area-preserving maps in the prediction of field line behaviour in a non-axisymmetric toroidal plasma containing device. We focus particularly on profiles of the rotational transform leading to the violation of the twist condition suggesting the application of nontwist maps. To the Heliac stellarator H-1 described by Hamberger *et al.* (1990) we apply the Hamiltonian formalism discussed by Gandy *et al.* (1993) for toroidal magnetic confinement systems generally and for torsatrons in particular. From this Hamiltonian formalism, following the discussions in Ott (1993) and of Lichtenberg and Lieberman (1992), we obtain area-preserving maps providing a convenient tool for analysis of the field-line dynamics. Fields with positive-definite shear have been well-studied with twist maps, but nontwist maps have only recently been applied to those with local minima or maxima (Hayashi *et al.* 1995).

A stellarator is a toroidal plasma containment device whose magnetic field is mainly generated by currents in windings external to the plasma. These external coils are designed so that, even with no plasma present, the magnetic field lines wrap around inside a toroidal vacuum vessel in such a way that they are everywhere tangential, or approximately tangential (Dewar *et al.* 1994), to a family of nested topologically toroidal surfaces, called 'magnetic flux surfaces'.

Stellarator puncture plots are ideal vehicles for the study of $1\frac{1}{2}$-degree of freedom Hamiltonian systems, since any such magnetic field line system is a

0004-9506/95/050871$05.00

realisation of a perfectly dissipation-free Hamiltonian flow (Cary and Littlejohn 1983; Boozer 1983; Yoshida 1994). The phase space (plus time) of our Hamiltonian system corresponds to the real space of the physical torus. A puncture plot is a physically realised Poincaré section of that phase space. A puncture plot is a plot of successive intersections, or 'punctures', by magnetic field lines of a cross-sectional surface cutting the physical magnetic torus everywhere transverse to the magnetic field. Puncture plots can be constructed directly from experiment using low-energy electron beams, or calculated by computer programs modelling stellarator field line behaviour either in the vacuum case or when perturbed by currents in a plasma.

Typically there exists a unique closed field line, the 'magnetic axis', that generates a fixed point on the puncture plot. This forms the centre of the family of toroidal magnetic surfaces referred to above. In the special case that the corresponding Hamiltonian system is *integrable*, the field lines within a finite volume are all perfectly tangential to toroidal magnetic surfaces. In general, this ideal case cannot be achieved precisely, but by careful design it can be arranged that the field line Hamiltonian is close to (weakly perturbed from) an integrable Hamiltonian. Then the Kolmogorov–Arnol'd–Moser (KAM) theorem (see e.g. Lichtenberg and Lieberman 1992) can be invoked to argue that there will still be a finite measure of perfect magnetic surfaces, with chaotic and island regions sandwiched in between them.

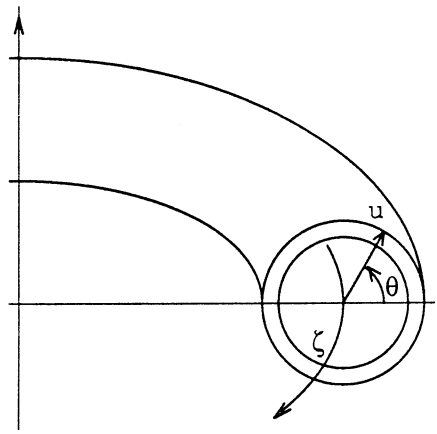

Fig. 1. Stylised flux-coordinate system showing the relations between the poloidal angle θ, the flux surface enumeration variable u, and the time-like angle ζ measured around the principal axis.

When the field is integrable, a generalised toroidal angle ζ measured approximately parallel to the magnetic axis, a poloidal angle θ period 2π measured about the magnetic axis, and a flux-surface-labelling quantity u can be found so as to form a canonical set of Hamiltonian action-angle variables. If one visualises an electron following a magnetic field line around its path with unit toroidal angular velocity, the toroidal angle ζ period 2π is a measure of time, the poloidal angle θ represents the angle variable of the action-angle pair, and u plays the role of the action, the momentum conjugate to θ (see Fig. 1). The use of such a curvilinear magnetic coordinate system has become a standard tool in the analysis of stellarator physics (D'Haeseleer *et al.* 1990). Even when the field is not integrable, a canonically conjugate pair (θ, u) with a corresponding 'perturbed' Hamiltonian can be found (Cary and Littlejohn 1983; Boozer 1983; Yoshida 1994).

Our system of a variable θ, its conjugate momentum-like variable u, plus the periodic time-like variable ζ, is said to form a Hamiltonian system of one and a half degrees of freedom. The half degree of freedom is time, here an angle variable in our three-dimensional (θ, u, ζ) phase space.

In Section 2 we develop the Hamiltonian formalism for stellarators, following the discussion of Gandy *et al.* (1993) for monotonically increasing rotational transform, and then extend the formalism to the zero-shear case. From the Hamiltonian formalism, we develop the general theory of the corresponding area-preserving maps in Section 3. In Section 4, we obtain the twist map (a form of the standard map) appropriate for the non-zero shear case and, in Section 5, the appropriate map for the nontwist case, one form of which is the standard nontwist map. Section 6 is the Conclusion. The Appendix discusses a useful transformation.

2. Hamiltonian Formalism

A time-independent N-degree of freedom Hamiltonian system is integrable if it has N independent global constants of the motion, one of which can be taken to be the Hamiltonian itself. This requirement implies the trajectory in phase space is restricted to an N-dimensional torus. Our Hamiltonian is given by the toroidal component of the vector potential of the magnetic field. Ideal stellarator field coils are designed to produce a toroidal magnetic field forming a compact set of uniform flux surfaces nested around the magnetic axis. Invariance of the surface integral of the flux through cross sections of the flux surface as we follow it around the toroidal axis is analogous to time-invariance of the Hamiltonian. Our system has $N = 1$. In augmented phase space, the two-dimensional torus to which ideal field-line motion is restricted for a particular Hamiltonian value is a tubular flux surface. Once a field line punctures a poloidal cross section of the physical torus on the flux surface for a particular Hamiltonian value, that field-line's successive punctures while orbiting the torus are restricted to the closed-curve intersection of the flux surface with the poloidal plane.

Our investigation begins with a nested set of ideal magnetic flux surfaces, closely approximated by design in actual stellarators (Shats *et al.* 1994). Any quantity constant on each surface and increasing monotonically from the magnetic axis outward can be used as a flux surface label u, though usually with $u = 0$ at the magnetic axis. With careful choice of coordinates we can write an unperturbed action-angle Hamiltonian (Gandy *et al.* 1993) as

$$H(u, \theta, \zeta) = H_0(u)\,, \tag{1}$$

that is, the Hamiltonian is constant everywhere on the flux surface labelled u, is independent of the angle θ, and is autonomous (independent of time). Note that we are not assuming the system to have any particular symmetry in physical space—the 'unperturbed' system may be strongly non-axisymmetric. Hamilton's equations of motion for a field line are here

$$\frac{\mathrm{d}u}{\mathrm{d}\zeta} = -\frac{\partial H}{\partial \theta} = 0\,, \tag{2}$$

$$\frac{\mathrm{d}\theta}{\mathrm{d}\zeta} = \frac{\partial H}{\partial u} = \iota(u)\,. \tag{3}$$

(The toroidal frequency is, by definition, unity.) In the dynamical systems literature ι is more commonly called the rotation number or winding number. The *rotational transform* ι is the time-like derivative of θ and therefore represents the natural poloidal frequency of the unperturbed system at a given u. For a given value of u, the variable θ increases by $\iota = 2\pi\iota$ each ζ-period. The increase is linear with ζ; hence θ and ζ are called straight field line coordinates. Plotted in the (ζ, θ) plane, field lines appear as straight lines.

In an integrable system, the magnetic field lines form a uniformly dense (with respect to θ) compact set on a given flux surface, and the tubular flux surfaces are densely nested between the magnetic axis and the plasma edge. A given flux surface can be characterised as rational or irrational by the value of the rotational transform ι. In general, ι is a continuous single-valued function of the flux-surface parameter u. If ι is irrational at a particular surface, one field/flux line will cover the surface with arbitrary density as it travels around the toroid an arbitrary number of times. If ι for a given surface, labelled u_r, has the rational value,

$$\iota(u_r) = \frac{n}{m}\,, \tag{4}$$

a resonance occurs when the head of a field line returns to its tail after m cycles around the toroidal axis with n twists around the magnetic axis. Covering the flux surface to an arbitrary density will require a number of separate field lines equal to the line integral of the density around the circumference of the flux surface divided by n times the density.

Because such surfaces are not structurally stable, in an actual stellarator, magnetic islands (centred on stable orbits) and regions of chaos exist, reflecting a less than ideal design or construction of the machine or the effect of currents arising spontaneously in the plasma. We assume here the imperfections produce small perturbations to the ideal Hamiltonian and hence to the ideal nested flux surface system. So the total Hamiltonian is the sum of the Hamiltonian for ideal nested surfaces and perturbations periodic in θ and ζ,

$$H(u, \theta, \zeta) = H_0(u) + \sum_{m,n} \epsilon_{mn}(u) \cos(m\theta - n\zeta - \eta_{mn}(u))\,, \tag{5}$$

where ϵ_{mn} and η_{mn} are the perturbation Fourier amplitudes and phases respectively. Since the perturbation has an explicit time-dependence, the perturbed system is non-autonomous and, in general, non-integrable. Resonance occurs when the frequency of the driving perturbation coincides with the natural frequency of the unperturbed Hamiltonian, that is, when the ratio of the summation indices n/m equals the value of ι at a rational surface.

Resonance produces magnetic island chains at the location of the unperturbed rational surface, though in a well-designed stellarator the individual islands in a high-order chain are numerous but small, so it can be difficult to distinguish a chain of islands from a smooth surface. While $n/m = 2/1$, $4/2$, and $6/3$ all represent the same value of ι, they represent different Fourier components with different phases and strengths produced by different deviations from ideal design of the field coils of an actual machine. Each will have a different number of islands

in its chain given by the denominator m. Less pronounced higher-order chains with the same n/m are presumably swallowed up by pronounced low-order chains, the higher n and m components merely producing small harmonic distortions on the basic island structure. Thus, unless forbidden by symmetry or removed by careful design, the dominant n and m will be the lowest, mutually prime, pair satisfying equation (4).

The number of islands in a chain and the value of ι determine the value of the numerator n by equation (4), and n reflects the stellarator's physical symmetry. In a 3-fold symmetric helical stellarator the magnetic torus itself is designed to wind about the magnetic axis three times, and the numerator n of a rational-valued ι is divisible by 3. Experimentally-observed island chains whose number of islands m and ι-value imply an n-value not divisible by 3 are due to error fields. The H-1 Heliac has 36 toroidal field coils evenly spaced in a helix about the central conductor, so we can also expect chains of islands whose m-number is given by 36 divided by ι.

Close to a rational surface at u_r, we can expand H_0 in a Taylor series about u_r:

$$H = H_{0r} + \iota_r(u-u_r) + \tfrac{1}{2}s_r(u-u_r)^2 + \tfrac{1}{3}t_r(u-u_r)^3 + \ldots + \sum_{mn} \epsilon_{mn,r}\cos[(m\theta - n\zeta) - \eta_{mn,r}]\,, \tag{6}$$

where the subscript r indicates evaluation at the surface $u = u_r$, $s_r \equiv \iota'(u_r)$ is the shear parameter, and $t_r \equiv \iota'(u_r)$ measures the rate of change of the shear at the surface. Note the need to distinguish carefully between t_r and ι_r. The analogue of the classical mechanics level of potential, H_0 does not affect the perturbation dynamics and can be ignored.

We here perform a canonical transformation from the old canonical variables (θ, u) to new canonical variables (Θ, J) with the generating function $F(\theta, J, \zeta) = (\theta - \iota\zeta)(J + u_r)$. We obtain, then, the relationships between the old and new coordinates as $J = u - u_r$ and $\theta = \Theta - \iota\zeta$.

We first consider the case where the shear parameter is not zero. We assume the third and higher order terms are small compared with the second order term of equation (6) and confine our interest to the latter plus the Fourier expansion terms. With a redefined u_r, our perturbation Hamiltonian can be written:

$$\tfrac{1}{2}s_r(u-u_r)^2 + \sum_{mn} \epsilon_{mn,r}\cos[m\Theta - (n - \iota_r m)\zeta - \eta_{mn,r}]\,. \tag{7}$$

Note that the time-like dependence vanishes for the subset of n and m values. We will set the new phase angle to agree with experiment below.

A particular (n, m) resonance geometry results from the fundamental or first harmonic mode of our Fourier expansion when field lines twist n times around the magnetic/poloidal axis while winding around the toroidal axis m times at the surface with rational $\iota = n/m$. For a given n-fold symmetry, the effects of higher order harmonics, specified by $(2n, 2m)$, $(3n, 3m)$, etc., will be masked by the lowest order term. Off-harmonic terms will not excite the n/m resonance. We

can limit the perturbation to the lowest order term in the expansion consistent with the conditions imposed by the symmetry of the stellarator and the value of ι at a particular flux surface.

Keeping only the lowest order Fourier term of equation (7), then we obtain the standard Hamiltonian for a pendulum,

$$\tfrac{1}{2}s_r J^2 + \epsilon_{m,r}\cos(m\Theta + \eta')\,, \tag{8}$$

with period $2\pi/m$ in Θ. We here choose the phase to produce an elliptical stability point ('O' point) at $\Theta = 0$ and, for computational convenience, pick the reference level of potential to re-write our perturbation Hamiltonian as

$$K = \tfrac{1}{2}s_r J^2 + \epsilon_{m,r}(1 - \cos m\Theta)\,. \tag{9}$$

From this we can plot the contour diagram shown in Fig. 2 for $m = 5$. Each level curve in Θ and J represents a different value of K. The partial Hamiltonian K is similar to that of a particle in a potential well. The separatrix is the level curve at the top of the well for which the total Hamiltonian value equals that of the unperturbed integrable flux surface. The oval-shaped contours within the separatrix are level curves for values of K less than that of the separatrix, the most negative of which, $K = -2\epsilon$, occurs at the elliptic periodic points at the centres of the islands.

We began with a time-dependent and therefore non-integrable perturbation Hamiltonian. By restricting the terms to lowest and transforming away the time-dependence, we have arrived at the Hamiltonian for a pendulum, which is integrable with constant value contour levels.

To obtain the ratio of the half-width (or half-height) to half-length of an island inside the separatrix, we first note at a given K that J will have a maximum value when the cosine contribution is unity ($\Theta = 0$):

$$K = \tfrac{1}{2}s_r(\delta J)^2\,. \tag{10}$$

Similarly the maximum angle $\delta\Theta$ will occur when the J contribution is zero:

$$K = \epsilon(1 - \cos m\delta\Theta)\,, \tag{11}$$

where $\epsilon = \epsilon_{m,r}$. Thus

$$J = \left(\frac{2K}{s_r}\right)^{\frac{1}{2}} = \left(\frac{2\epsilon(1 - \cos m\delta\Theta)}{s_r}\right)^{\frac{1}{2}}, \tag{12}$$

or, dividing by $\delta\Theta$,

$$\frac{\delta J}{\delta\Theta} = \left[\frac{2e(1 - \cos m\delta\Theta)}{s_r(\delta\theta)^2}\right]^{\frac{1}{2}}, \tag{13}$$

which approaches $m(\epsilon/s_r)^{\frac{1}{2}}$ as $\delta\Theta \to 0$.

The full-width of the island chain can be defined as the maximum full-width of the separatrix (when $\Theta = 0$ and $m\delta\Theta = \pi$),

$$\Delta J = 2\delta J = 4\left(\frac{\epsilon}{s_r}\right)^{\frac{1}{2}}. \tag{14}$$

The width is proportional to the square root of the perturbation strength, in agreement with Gandy *et al.* (1993).

To better show that the perturbation Hamiltonian equation (9) represents a chain of islands, the contour diagram of Fig. 2 is replotted in the polar diagram of Fig. 3*a*. For easier comparison with actual puncture plots and the plots produced by field-line tracing programs, we incorporate a chain of islands predicted by this simple model into a nest of flux surfaces plotted in the shape of a bean using a parametrisation scheme (discussed in the Appendix) in Fig. 3*b* and compare it with a field line tracing program puncture plot in Fig. 4.

Fig. 2. Hamiltonian 5-island chain.

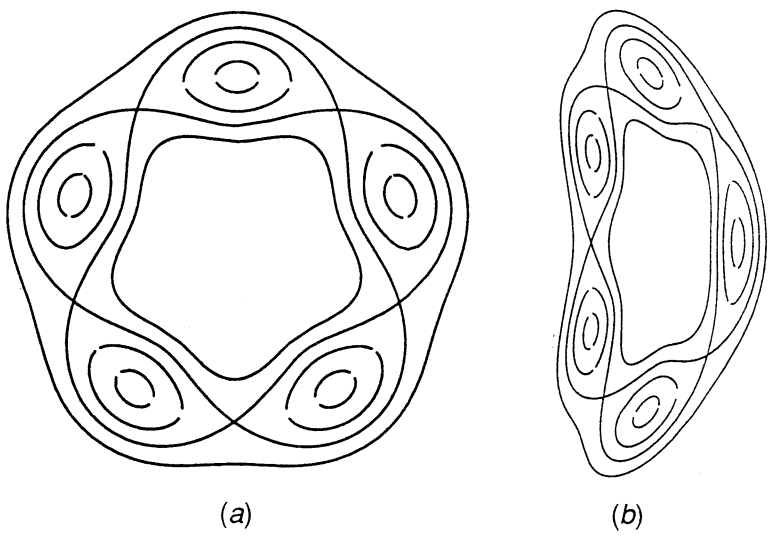

Fig. 3. Island chain of Fig. 2 plotted in a circle (*a*) and transformed into a bean shape (*b*).

When the rotational transform ι has a maximum or a minimum, its first derivative, the shear coefficient, vanishes. The Hamiltonian expansion (6) then has no second order term. Expanding the Hamiltonian about u_r and keeping only the lowest-order perturbation terms again, we have

$$H = H_{0r} + \iota_r(u - u_r) + \tfrac{1}{3}\iota_r(u - u_r)^3 + \ldots + \epsilon_{m,r}\cos(m\theta - n\zeta)\,, \qquad (15)$$

which is odd in $(u - u_r)$. Again we can define away the first two terms and neglect fourth and higher order terms, but we keep the third order term to obtain a perturbation Hamiltonian

$$K = \tfrac{1}{3} t_r J^3 - \epsilon_{m,r}(1 - \cos m\Theta)\,. \tag{16}$$

Contours of this Hamiltonian are plotted in Fig. 5 for $K = 0$ and are consistent with the reconnection scenario for the logistic twist map of Howard and Hohs (1984) and the nontwist map of del-Castillo-Negrete and Morrison (1993).

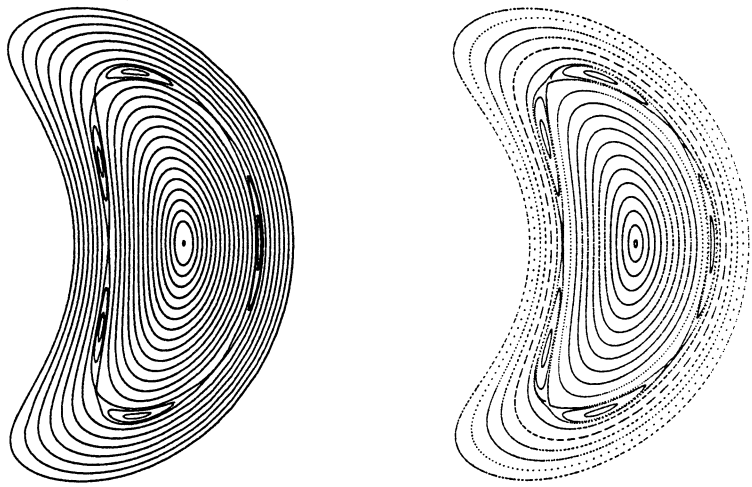

Fig. 4. Bean-shaped island chain of Fig. 3*b* with reduced perturbation parameter embedded in nested flux surfaces (*a*) for comparison with puncture plot (*b*).

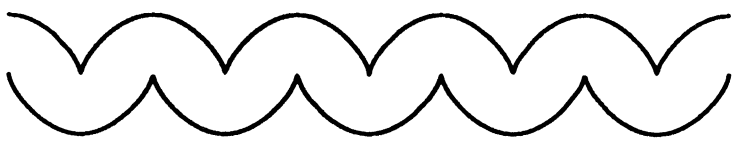

Fig. 5. Reconnected 5-island chain when the Hamiltonian has zero shear.

3. Area-preserving Maps

The discretised versions of Hamilton's equations (2) and (3) for the perturbed Hamiltonian of equation (9) are

$$\frac{\Delta u}{\Delta \zeta} = \frac{u_{n+1} - u_n}{2\pi} = -\epsilon \sin m\theta_n\,, \tag{17}$$

$$\frac{\Delta \theta}{\Delta \zeta} = \frac{\theta_{n+1} - \theta_n}{2\pi} = t(u_{n+1})\,. \tag{18}$$

Note the time-sequence subscript n here is not the same as the n of the rational number n/m, and we have dropped the now unnecessary r-and m-subscripts from ϵ. Without perturbation, u is constant and θ increases linearly with time.

The above equations can be recast in the form of a map by writing them as, respectively,

$$u_{n+1} = u_n - 2\pi\epsilon \sin m\theta_n \,, \tag{19}$$

$$\theta_{n+1} = \theta_n + 2\pi t(u_{n+1}) \,. \tag{20}$$

The Jacobian of the map defined by equations (19) and (20) is

$$\begin{vmatrix} \partial\theta_{n+1}/\partial\theta_n \,, & \partial\theta_{n+1}/\partial u_n \\ \partial u_{n+1}/\partial\theta_n \,, & \partial u_{n+1}/\partial u_n \end{vmatrix} = \left[1 + 2\pi t'(u_{n+1})\frac{\partial u_{n+1}}{\partial\theta_n}\right] - 2\pi t'(u_{n+1})\frac{\partial u_{n+1}}{\partial\theta_n}$$

$$\equiv 1 \,. \tag{21}$$

Thus the map is, quite generally, area preserving.

For computational simplicity we re-define the poloidal angle θ to have period one-revolution about the magnetic axis, and re-define the perturbation parameter ϵ dividing it by 2π. We then rewrite equations (19) and (20) as

$$u_{n+1} = u_n - \epsilon \sin 2\pi m\theta_n \,, \tag{22}$$

$$\theta_{n+1} = \theta_n + t(u_{n+1}) \,. \tag{23}$$

We can subtract u_r from both sides of equation (22) and replace $u - u_r$ on both sides by J to obtain

$$J_{n+1} = J_n - \epsilon \sin 2\pi m\theta \,. \tag{24}$$

Similarly we can expand t about $u = u_r$ to obtain

$$\theta_{n+1} = \theta_n + t(u_r) + t'(u_r)J_{n+1} + \tfrac{1}{2}t''(u_r)J_{n+1}^2 + \ldots$$

$$\equiv \theta_n + t_r + sJ_{n+1} + \beta J_{n+1}^2 + \ldots \,, \tag{25}$$

where we have defined $s \equiv t'(u_r)$ and $\beta \equiv \frac{1}{2}t''(u_r)$.

4. Twist Maps

Assuming t is roughly linear with a non-zero slope (s non-zero), equations (24) and (25) are the equations for a twist map. The map represents flux lines on one surface twisted relative to those on adjacent surfaces. The map is a radial twist map if θ is periodic. The radial twist map form of our area-preserving map can be written as

$$J_{n+1} = J_n - \epsilon \sin 2\pi m\theta \,, \tag{26}$$

$$\theta_{n+1} = \theta_n + t_r + sJ_{n+1} \,. \tag{27}$$

Equations (26) and (27) are one form of the standard map used to plot Fig. 6, which can be compared with the island chains of Figs 2–4.

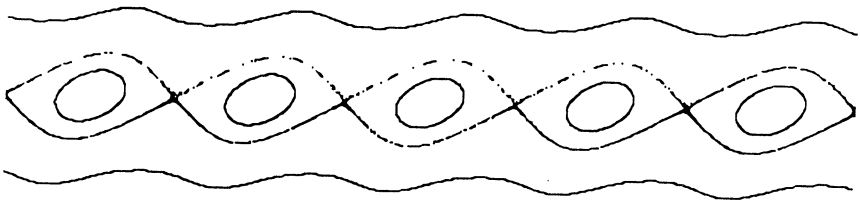

Fig. 6. Chain of 5 islands predicted by standard map.

5. Nontwist Maps

When the twist condition is violated [the shear coefficient $\iota'(u_r)$ is zero], our area-preserving map takes the form:

$$J_{n+1} = J_n - \epsilon \sin 2\pi m\theta_n \,, \tag{28}$$

$$\theta_{n+1} = \theta_n + \iota_r + \beta J_{n+1}^2 \,. \tag{29}$$

With β restricted to $\beta = -\iota_r$, these equations are the standard nontwist map of del-Castillo-Negrete and Morrison (1993), also studied by Weiss (1991) and compared with pressure-broadened heliac plots by Hayashi *et al.* (1995).

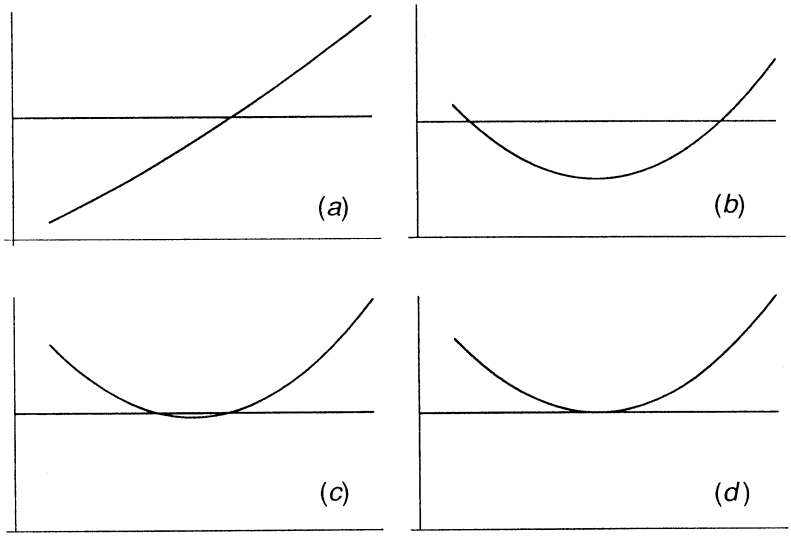

Fig. 7. Possible ι curves considered in this work plotted (along the vertical axis) against flux-surface enumeration variable u (along the horizontal axis) with (*a*) ι monotonically increasing and crossing a rational value in the middle of the flux-surface nest, (*b*) ι having a local minimum well below the rational value of interest, (*c*) ι having a local minimum just below a rational value, and (*d*) ι having a local minimum at a rational value.

In Figs 7*a–d* we plot four arbitrary ι curves of interest in the present work as a function of the surface parameter u in the vicinity of a rational value $\iota = n/m$. In Fig. 7*a* ι is a monotonic function of u near the value n/m. This would be the case for the classic twist map of a single chain of m islands. A chain

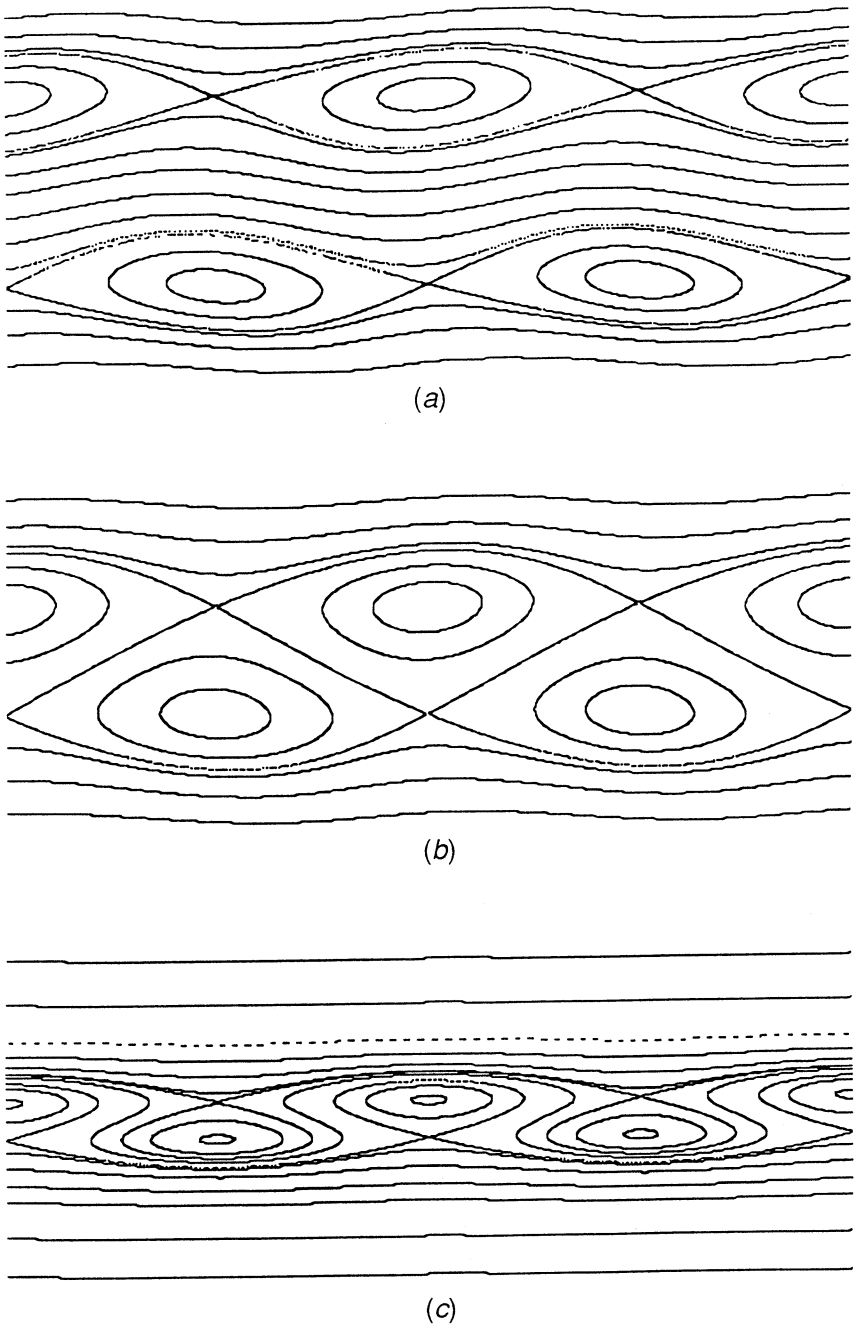

Fig. 8. Nontwist maps (a), (b) and (c) topologically similar to puncture plots expected when ι has a functional dependence and values similar to those illustrated in Figs 7b, 7c and 7d respectively.

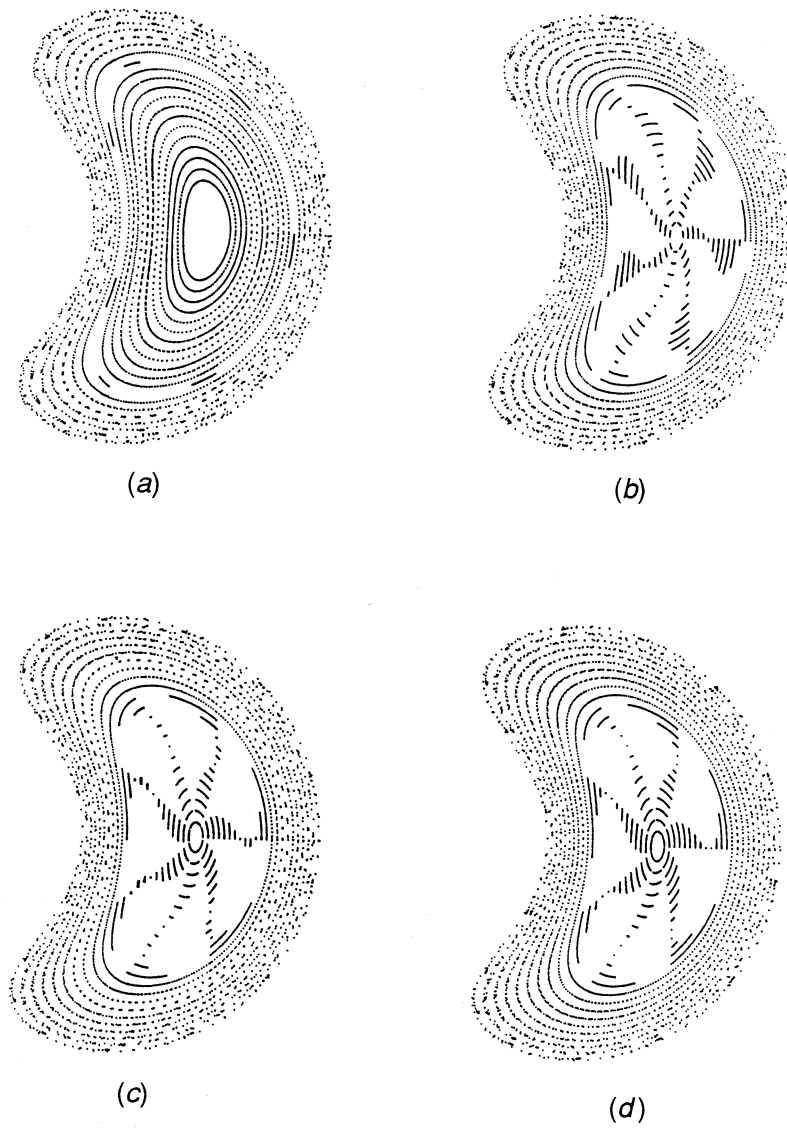

Fig. 9. Puncture plots (a–d) where ι is evolving approximately as in Figs 8a–d respectively. Here the perturbation is small and the topological details of the islands are not visible at this scale. The histogram-like images along the right symmetry axes in the plots show roughly the differences between ι and the rational value $\frac{9}{7}$. Chains of seven islands are expected where the ι histogram curves cross the symmetry axis. These would be the locations of stable orbits with no perturbation.

similar to that of Fig. 5 might have $\iota = 1{\cdot}2$, $n = 6$ and $m = 5$, for example. In Fig. 7b we show a roughly parabolic ι curve having its minimum well below the n/m rational value. Each crossing by the ι curve of the line drawn at constant $\nu n/m$ would result in a chain of m islands, and we would construct a

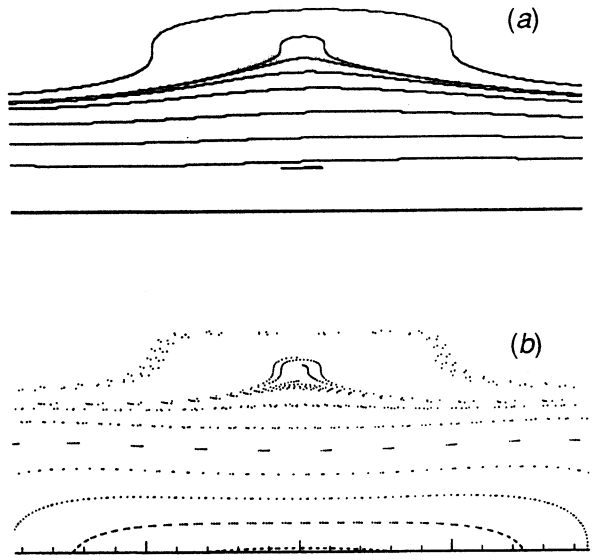

Fig. 10. A detail from a nearly re-connected $m = 2$ puncture plot is shown in (a) for comparison with the appropriate nontwist map in (b).

separate approximate Hamiltonian in each of the two cases. We would use the same twist map equations (26) and (27) in each case, each producing a chain of the same number of magnetic islands. The two island chains would each be similar to that of Fig. 5. By contrast if the ι curve minimum occurs close to or at the value n/m, as in Figs 7c and 7d, the twist condition is violated, at least approximately, and it is appropriate to use the standard nontwist map of equations (28) and (29). The two cases will result in plots similar to those of Figs 8a and 8b respectively. Nontwist maps become appropriate as the distance in the u-direction between two island chains of equal m-number approaches the width of the islands in the chains.

In Figs 9a–d we show a series of puncture plots predicted by a Heliac vacuum field line tracing program, the Gourdon code (Gourdon *et al.* 1971), to match the series of conditions of Figs 7a–d for $m = 7$. We show a puncture plot in Fig. 10a produced by the nontwist map of equations (28) and (29), choosing parameters for visual agreement with the predictions of a field line tracing computer program shown in Fig. 10b.

6. Conclusion

The existence of nested flux surfaces in a stellerator implies a canonical Hamiltonian relationship among the variables describing the location of the intersection of a flux surface with a poloidal cross section. It also implies the existence of an integrable Hamiltonian. Without knowing the physical origin of

this Hamiltonian or its explicit dependence on the canonical variables, we can infer a perturbation Hamiltonian which approximately describes magnetic island chains in analytic form and provides some insight into perturbation strengths and the value of the rotational transform at a particular puncture plot location. From the Hamiltonian description we can derive a description of the same phenomena using area-preserving maps. Where the rotational transform ι does not have a local minimum at the location of an unperturbed rational flux surface (the non-zero shear case), we use a twist map. Where the shear vanishes (ι has a local minimum), a nontwist map is appropriate. It would be interesting to use the results of the present work to examine the relation between island sizes, the shape of the ι curve and perturbation strengths and to explore the evolution of Hamiltonian maps from twist to nontwist cases as we vary the shape of the ι curve.

Acknowledgments

One of us (MGD) wishes to acknowledge the kind support of the Australian National University while he was there on professional leave during 1994, especially for discussions with Boyd Blackwell and for the data and computational help he provided. We ran the Gourdon field-line tracing program (Gourdon *et al.* 1971) on the Fujitsu VP2200 at the Australian National University Supercomputer Facility. The Hamiltonian plots were made with Mathematica (Wolfram 1991) and the map plots with the Cornell University modelling package dstool (Guckenheimer *et al.* 1993).

References

Boozer, A. H. (1983). *Phys. Fluids* **26**, 1288.
Cary, J. R., and Littlejohn, R. G. (1983). *Ann. Phys. (NY)* **151**, 1.
Chance, M. S., Jardin, S. C., and Stix, T. H. (1983). *Phys. Rev. Lett.* **51**, 1963.
del-Castillo-Negrete, D., and Morrison, P. J. (1993). *Phys. Fluids* A **5**, 948.
Dewar, R. L., Hudson, S. R., and Price, P. F. (1994). *Phys. Lett.* A **194**, 49.
D'Haeseleer, W. D., Hitchon, W. N. G., Callen, J. D., and Shohet, J. L. (1990). 'Flux Coordinates and Magnetic Field Structure' (Springer: New York).
Gandy, R. F., Hartwell, G. J., Hanson, J. D., Knowlton, S. F., and Lin, H. (1993). *Phys. Fluids* B **5**, 4384.
Gourdon, C., Marty, D., Maschke, E. K., and Touche, J. (1971). *Nucl. Fusion* **11**, 161.
Guckenheimer, J., Myers, M. R., Wicklin, F. J., and Worfolk (1993). '`dstool`: A dynamical system toolkit with an interactive graphical interface' (Center For Applied Mathematics: Cornell University).
Hamberger, S. M., Blackwell, B. D., Sharp, L. E., and Shenton, D. B. (1990). *Fusion Technology* **17**, 123.
Hayashi, T., Sato, T., Gardner, H. J., and Meiss, J. D. (1995). *Phys. Plasmas* **2**, 752.
Howard, J. E., and Hohs, S. M. (1984). *Phys. Rev.* A **29**, 418.
Lichtenberg, A. J., and Lieberman, M. A. (1992). 'Regular and Chaotic Motion' (Springer: New York).
Monticello, D. A., Dewar, R. L., Furth, H. P., and Reiman, A. (1984). *Phys. Fluids* **27**, 1248.
Ott, E. (1993). 'Chaos in Dynamical Systems' (Cambridge University Press: New York).
Shats, M. G., Rudakov, D. L., Blackwell, B. D., Sharp, L. E., Tumlos, R., Hamberger, S. M., and Fedyanin, O. I. (1994). *Nucl. Fusion* **34**, 1653.
Weiss, J. B. (1991). *Phys. Fluids* A **5**, 1379.
Wolfram, S. (1991). 'Mathematica', 2nd edn (Addison–Wesley: Redwood City, Ca).
Yoshida, Z. (1994). *Phys. Plasmas* **1**, 1.

Appendix: Bean-shape Parametrisation

The bean-shape parametrisation scheme described here is an intuitive way of visualising the transformation between flux coordinates and physical space. The scheme is similar to the more commonly used bean-shape parametrisation scheme described by Chance *et al.* (1983) and by Monticello *et al.* (1984), except that our transformation is easier to apply to the magnetic islands arising from Hamiltonian theory, is analytically invertible, provides an excellent fit to experiment, and is easier to visualise.

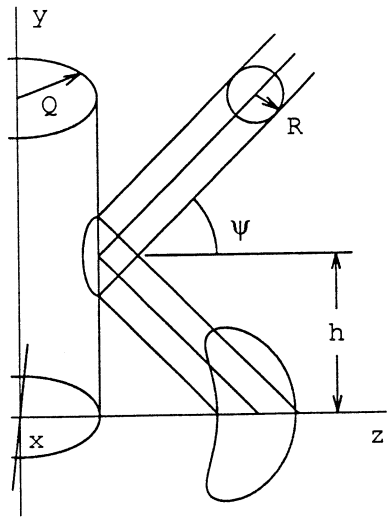

Fig. 11. Circular light beam incident on a vertical reflecting circular cylinder of larger radius to produce a bean shape on the underlying horizontal surface.

The mapping is inspired by the optical transformation obtained on reflecting a circular beam of light in an upright circular cylinder onto its base plane. The circular beam (of radius R) with its central ray ($R = 0$ ray) in the (y, z)-plane is directed at an angle of incidence ψ toward a circular reflecting cylinder (of radius $Q > R$) whose symmetry axis is the y-axis (see Fig. 11). The circular beam of light will be reflected onto the (x, z)-plane, its image bean-shaped with its centre falling on the z-axis at a distance $Q + h/\tan\psi$ from the y-axis, where h is the height at which the central ray strikes the cylinder. While still capturing the intuitive features of the model, the equations given below for the transformation have been modified in order to simplify the inverse mapping, which otherwise involves the recovery of the roots of a quartic equation. If we fill the circular beam with a nest of circular surfaces, the reflected image is a nest of bean-shaped surfaces which closely mimic the nested surfaces found experimentally. If we describe a point in a cross-section of the circular beam by the polar coordinates (R, Θ), the transformation to the (x, z) coordinates of the corresponding point in the bean-shaped image is written as:

$$x = D\cos\phi, \tag{30}$$

$$z = D\sin\phi, \tag{31}$$

where the intermediate variables D and ϕ are defined by

$$D = Q\sin\phi + \frac{h + R\sin\Theta}{\tan\psi}, \tag{32}$$

$$Q\cos\phi = R\cos\Theta. \tag{33}$$

The shape of the bean is determined by the fitting parameters ψ and Q. We can also adjust the height h to adjust the bean's overall size.

The centre of the bean can represent the magnetic axis of a bean-shaped puncture plot. The corresponding (r, θ) polar coordinates centred on the magnetic axis are given with $(x, z') = (x, z - Q - z_0)$ as

$$r = (x^2 + z'^2)^{\frac{1}{2}}, \tag{34}$$

$$\theta = \arctan\frac{x}{z'}, \tag{35}$$

where θ is the usual poloidal angle defined in the Introduction. Equations (30)–(35) thus define a mapping from the 'flux coordinates' (R, Θ) to the 'real space' coordinates (r, θ).

Manuscript received 28 November 1994, accepted 30 March 1995